MethodsX 11 (2023) 102253

Contents lists available at ScienceDirect

MethodsX

journal homepage: www.elsevier.com/locate/mex

# Constructing a model including the cryptic sulfur cycle in Chesapeake Bay requires judicious choices for key processes and parameters ☆

Rui Jin [a,*], Marie-Aude Pradal [a], Kalev Hantsoo [a], Anand Gnanadesikan [a], Pierre St-Laurent [b], Christian J. Bjerrum [c]

[a] Department of Earth and Planetary Sciences, Johns Hopkins University, Baltimore, MD 21218, United States
[b] Virginia Institute of Marine Science, William & Mary, Gloucester Point, VA 23062, United States
[c] Department of Geoscience and Natural Resource Management, University of Copenhagen, Copenhagen 1165, Denmark

ARTICLE INFO

*Method name:*
SNP_BUR_DOM

*Keywords:*
Modeling predictions
Hypoxia
Particle sinking
Nitrification
Stoichiometry
Optics absorption

ABSTRACT

A new biogeochemical model for Chesapeake Bay has been developed by merging two published models – the ECB model of Da et al. (2018) that has been calibrated for the Bay but only simulates nitrogen, carbon and oxygen and the BioRedoxCNPS model of al Azhar et al. (2014) and Hantsoo et al. (2018) that includes cryptic sulfur cycling. Comparison between these models shows that judicious choices are required for key processes and parameters. This manuscript documents the sources of differences between the two published models in order to select the most realistic configuration for our new model.

- This study focuses on three sets of differences–processes only included in ECB (burial and dissolved organic matter), processes only included in BioRedoxCNPS (explicit dynamics for hydrogen sulfide, sulfate and nitrite, light attenuation that does not include CDOM or sediments), and differences in parameters common to the two codes.
- Sensitivity studies that highlight particular choices (absorption by dissolved organic matter, nitrification rates, stoichiometric ratios) are also shown.
- The new model includes sulfur cycling and has comparable skill in predicting oxygen as ECB, but also has improved simulation of nitrogen species compared with both original codes.

## Specifications table

| | |
|---|---|
| Subject area: | Environmental Science |
| More specific subject area: | *Oceanographic modeling* |
| Name of your method: | *SNP_BUR_DOM* |
| Name and reference of original method: | *ECB-Da et al. (2018), BioRedoxCNPS-al Azhar et al. (2014),* Hantsoo et al. (2018) |
| Resource availability: | ⟨13:italic ⟩https://github.com/RuiJinSZ/Merged-Model-MethodsX⟨/13:italic⟩ |

☆ Related research article Jin, R., Pradal, M., Hantsoo, K., Gnanadesikan, A., St-laurent, P., 2023. Comparing two ocean biogeochemical models of Chesapeake Bay with and without the sulfur cycle instead highlights the importance of particle sinking, burial, organic matter, nitrification and light attenuation. Ocean Model. 182, 102175. *https://doi.org/10.1016/j.ocemod.2023.102175*

* Corresponding author.
*E-mail address:* ruijin@jhu.edu (R. Jin).

https://doi.org/10.1016/j.mex.2023.102253
Received 14 March 2023; Accepted 10 June 2023
Available online 11 June 2023

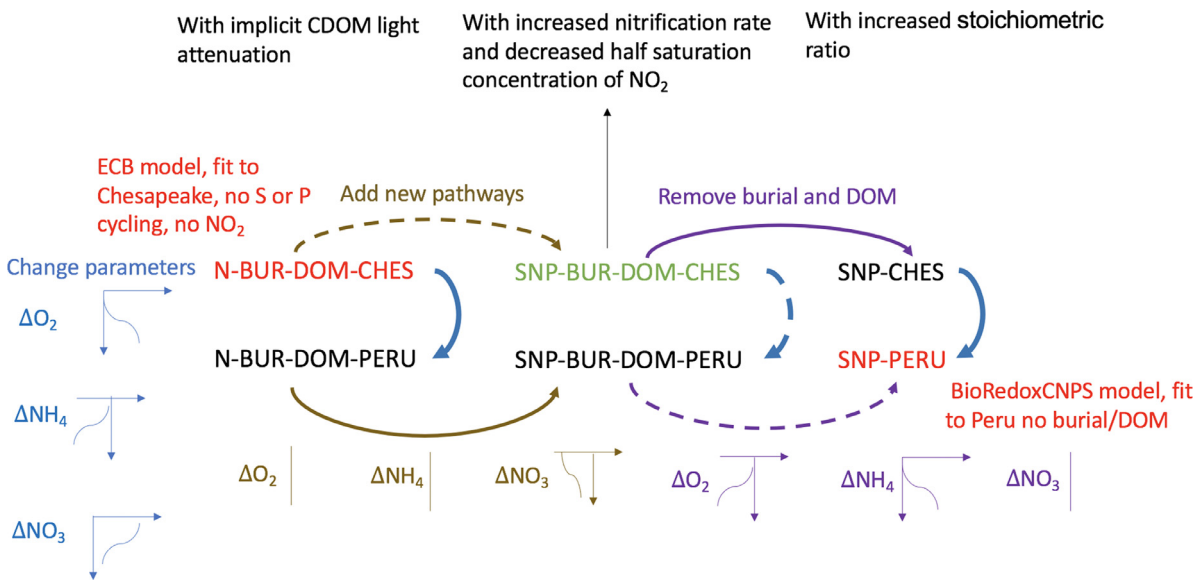


**Fig. 1.** Diagram illustrating the results presented in this paper. Arrows show pathways for transforming the ECB code as configured in Da et al. [5] (N_BUR_DOM_CHES) to the BioRedoxCNPS code as configured in Hantsoo et al. [8] (SNP_PERU). Two previously published models are shown in red. The reference run from the merged model in this paper is shown in green. The other runs are shown in black. The thick blue arrows indicate the differences in parameters common to both models. The purple lines indicate removing burial and DON. The brown lines indicate adding sulfur and phosphorus cycling. The resulting changes to oxygen, ammonium and nitrate profiles are shown schematically next to each set of changes. Three sensitivity studies using SNP_BUR_DOM_CHES as a control are shown at the top of the diagram.

## Method details

### *Background*

Over recent decades, much effort has been made to study hypoxia in Chesapeake Bay, including the development of a number of numerical models. Chesapeake Bay is a prominent estuary located on the East Coast of the United States, encompassing parts of Maryland and Virginia. It is the largest estuary in the country and plays a crucial role in providing habitat for numerous species, contributing to fisheries, and serving as a valuable recreational resource for surrounding communities. Da et al. [5] implemented a nitrogen-based model (referred to in that paper as ECB, in this paper as N_BUR_DOM_CHES) that can simulate oxygen skillfully in Chesapeake Bay. This model is currently used for hindcast studies of the Bay at the Virginia Institute of Marine Science and is also used to evaluate the impact of changes in nutrient delivery to the Bay. However, as shown both here and in the companion manuscript [10], this model has large biases when simulating certain nitrogen species. Additionally, it does not simulate a number of chemical species and processes which have been hypothesized to play an important role in the Bay. One such chemical species is hydrogen sulfide, which a number of studies have found to be present in the water column of the Bay [4,13]. There is evidence from other ecosystems that simulating sulfide oxidation as well as cryptic sulfur cycling (which involves tightly coupled sulfate reduction and sulfide oxidation without a buildup of hydrogen sulfide) might help to mitigate biases in simulating nitrogen species [3]. Bacteria capable of metabolizing hydrogen sulfide have been shown to be common in Chesapeake Bay with their abundances increasing in the presence of hypoxia [1]. Additionally, N_BUR_DOM_CHES does not simulate nitrite, which means that it cannot simulate anammox or sulfide oxidation by nitrite. Al Azhar et al. [2] constructed a model (referred to as BioRedoxCNPS in that paper) that includes hydrogen sulfide and nitrite and simulates sulfate reduction, sulfide oxidation by nitrite, nitrate and oxygen, anammox, two-stage denitrification and heterotrophic denitrification within the Peru Upwelling. This model matches observations of oxygen, nitrite, nitrate and phosphate as well as being broadly consistent with (low-precision) observational estimates of sulfate reduction, anammox and denitrification. An updated version of this code (with a number of improvements) was published by Hantsoo et al. [8].

This paper documents the construction of a model including the sulfur cycle that can simulate oxygen, nitrate and ammonium skillfully in Chesapeake Bay. As the first step, the model from al Azhar et al. [2] calibrated for the Peru Upwelling is implemented in the same physical model of Chesapeake Bay as the previously published N_BUR_DOM_CHES model of Da et al. [5]. The new model (referred to here as SNP_PERU), improves some fields but not others relative to N_BUR_DOM_CHES. This motivated us to develop a merged version of the two biogeochemical codes, run them in the same physical model and configure them so as highlight specific differences between the two published models (see Fig. 1, also the graphical abstract). Based on this analysis, a specific model configuration is picked as a basis for further development. Next, a set of sensitivity studies was conducted to further improve the model skill. Finally, we propose a reference model that can simulate oxygen, hypoxic volume, nitrate and ammonium more skillfully

**Table 1**
Summary of how the classes of model differences (common parameters, pathways seen one of the original codes) map onto our model simulations.

| Model | Include S, $NO_2$, Annamox | Implicit CDOM in light attenuation | Common Parameters | Burial and DOM | Remineralization: $NO_2$ to $NH_4$ |
|---|---|---|---|---|---|
| N_BUR_DOM_CHES (ECB) | N | Y | CHES | Y | Implicit ∞ |
| SNP_BUR_DOM_CHES | Y | N | CHES | Y | slow |
| SNP_BUR_DOM_PERU | Y | N | PERU | Y | slow |
| SNP_PERU(BioRedoxCNPS) | Y | N | PERU | N | slow |
| N_BUR_DOM_PERU | N | Y | PERU | Y | Implicit ∞ |
| SNP_CHES | Y | N | CHES | N | slow |

than either of the previously published models that can serve as a basis for future studies. A comparison table summarizing the different versions of the model can be found in the companion Ocean Modelling manuscript [10] as Table 2.

*Physical component of the model*

The physical component of our model is based on the Regional Ocean Modeling System (ROMS, [17]) which uses an orthogonal curvilinear grid with variable horizontal resolution. The highest resolution (430 m) is found in the northern Bay, the lowest resolution (~10 km) in the southern end of the Mid-Atlantic Bight, and the average grid spacing within the Chesapeake Bay is 1.7 km. The map displaying the model bathymetry as well as the locations of monitoring stations can be found as Fig. 1 in Jin et al. [10]. Governing equations are discretized over a stretched terrain-following s-coordinate with 20 vertical levels. To interpolate between a higher resolution in the surface and the bottom boundary layers in deeper waters and relatively constant resolution in shallow waters, the stretching function of Shchepetkin & McWilliams [16] was used with values $\theta$s=6.0 and $\theta$b=4.0 (standard values in this version of ROMS) with an hc = 10 m.

Tidal constituents were adopted from the Advanced Circulation (ADCIRC) model [12] and from observed nontidal water levels from Duck, NC and Lewes, DE [15]. They were imposed on the model at the open boundary. Atmospheric forcings, including winds, air temperature, relative humidity, pressure, precipitation, short-wave radiation and longwave radiation, were obtained from the North American Regional Reanalysis (originally described in [14]).

The MPDATA 3-D advection scheme [18,19] was used for tracers. MPDATA 3-D is a third-order upstream advection scheme that ensures that advection does not generate spurious maxima or minima while minimizing numerical diffusion (this is particularly important for biogeochemical tracers). Momentum is advected with a third-order centered difference scheme in the horizontal and fourth-order centered difference in the vertical. The vertical turbulent mixing scheme and background mixing coefficients for both momentum and tracers were all set to the same values as in Feng et al. [6].

*Biogeochemical cycling (BGC) codes and simulation setups*

We examined the behavior of three biogeochemical codes (ECB, BioRedoxCNPS, and our merger of the two: SNP_BUR_DOM), which we implemented using two parameter sets for phytoplankton growth, coagulation and sinking governed by equations in common to the two codes. One parameter set is taken from the Da et al. [5] model of the Chesapeake and the other is taken from the al Azhar et al. [2] model of the Peru upwelling system as modified by Hantsoo et al. [8]. Our experimental design thus contains six core simulations with two parameter sets implemented for each code. We use a nomenclature that makes it evident what *chemical species (N vs. S, N and P)* are cycled, whether the model includes *burial and DOM,* and whether the *parameter set* is taken from the Peru simulation or the Chesapeake simulation. N_BUR_DOM_CHES thus describes ChesROMS_ECB which cycles N but not S or P, includes burial and DOM, and uses parameters from Da et al. [5] for (among other things) sinking and phytoplankton growth. By contrast SNP_PERU describes our implementation of BioRedoxCNPS, with sulfur and phosphate cycling but no burial or DOM and uses parameters from Hantsoo et al., [8]. A more complete description of each simulation is given below and the differences are summarized in Table 1.

*N_BUR_DOM_CHES*

The BGC code in the N_BUR_DOM_CHES simulation is the same as the code used in Da et al. [5], which is derived from a nitrogen-based ecosystem code [7]. This code includes a simplified nitrogen cycle with 8 nitrogen pools (listed with model acronyms): nitrate ($NO_3$), ammonium ($NH_4$), phytoplankton (P), zooplankton (Z), semilabile and refractory dissolved organic nitrogen (DONsl and DONrf) and small and large nitrogen detritus (SDeN and LDeN). Additionally, the code simulates semilabile and refractory DOC (DOCsl and DOCre), inorganic suspended solids (ISS), chlorophyll (Chl), dissolved inorganic carbon (DIC), alkalinity (Alk), and dissolved oxygen ($O_2$). As implemented in the ChesROMS_ECB model, phytoplankton growth is limited by nitrogen and light and the dominant phytoplankton loss is via coagulation and sinking. The resuspension of fractions of phytoplankton and large detritus into small detritus upon reaching the bottom is influenced by the near-bottom turbulent velocities. Some fraction of the remaining benthic flux is buried permanently following the formula of Henrichs and Reeburgh [9] while the remainder undergoes remineralization.

$$f_{bur} = \min\left(0.75, 0.023 * carbon\ flux\ to\ the\ bottom^{0.5797}\right) \quad (1)$$

The carbon flux to the bottom is in units of mmol C/$m^2$/day. This means that when the flux of carbon is much less than ~400 mmol C/$m^2$/day most of the flux is remineralized. At low levels of flux to the bottom, doubling the flux results in a tripling of burial.

In this model, there are three pathways involved in transforming the organic material to inorganic nitrogen: 1. Solubilization of excreted materials produces DON. Both DON and detrital materials are remineralized to $NH_4$, 2. using oxygen if it is available and 3. nitrate (resulting in denitrification) if it is not.

*SNP_PERU*

The second biogeochemical simulation, SNP_PERU, uses the code developed by al Azhar et al. [2] and updated by Hantsoo et al. [8] to capture interactions between the cycles of nitrogen, phosphorus and sulfur in the Peru coastal ocean upwelling system. Like the ECB code, this code was also derived from the BGC code of Fennel et al. [7], and it has previously been referred to as BioRedoxCNPS [2] and Fennel_CNPS [8]. We refer to the unaltered version of this code implemented in the ChesROMS physical model domain with BGC parameters from Hantsoo et al. [8] as the SNP_PERU simulation. This code adds new explicit kinetic processes to the Fennel BGC code, described by the following set of equations:

$$(CH_2O)_{106}(NH_3)_{16}H_3PO_4+53H_2SO_4+11H^+ \rightarrow 106CO_2+53H_2S+16NH_4+H_2PO_4+106H_2O \quad (2)$$

$$H_2S+2O_2 \rightarrow 2H^++SO_4{}^{2-} \quad (3)$$

$$2H_2S+8NO_3{}^-+2H^- \rightarrow 8NO_2{}^-+2SO_4{}^{2-}+4H^+ \quad (4)$$

$$3H_2S+8NO_2{}^-+2H^- \rightarrow 4N_2{}^-+3SO_4{}^{2-}+4H_2O \quad (5)$$

1. Sulfate is reduced to $H_2S$ during organic matter remineralization when other oxidants (oxygen and nitrate) are limiting (Eq. 2). Sulfide is reoxidized to sulfate 2. by oxygen (Eq. 3), 3. by nitrate reduction to nitrite through chemolithoautotrophic nitrate reduction (Eq. 4) or 4. by nitrite reduction to $N_2$ gas through sulfide-driven denitrification (Eq. 5). When the water is anoxic, ammonium can also be oxidized by nitrite through anammox to produce $N_2$ gas. The SNP simulations used in this study thus include six state variables not included in N_BUR_DOM_CHES: nitrite ($NO_2$), sulfate ($SO_4$), hydrogen sulfide ($H_2S$), phosphate ($PO_4$) and small and large detrital phosphorus (SDeP, LDeP). Autotrophic nitrogen fixation by diazotrophs (which was included in the original study of al Azhar et al. [2]) was turned off in our simulations as it resulted in numerical instability and is not expected to play a major role in Chesapeake nitrogen dynamics given the excess of fixed nitrogen over phosphorus. It is notable that there are no sedimentary burial processes in the SNP code so that all organic materials hitting the bottom are remineralized. Thus, in comparison to N_BUR_DOM_CHES, SNP_PERU has two new *pathways* (anammox and sulfide-driven denitrification) by which nitrogen is lost to the system, but it simultaneously neglects the loss of nitrogen via burial. Additionally, dissolved organic materials are not included in this model. Finally, as described in Table 1 of the companion manuscript, although the equations for phytoplankton growth, grazing, coagulation, and detrital sinking can be cast in identical forms in SNP_PERU and N_BUR_DOM_CHES, many of the parameters within these equations are different in these two models. In particular, grazing and remineralization rates in N_BUR_DOM_CHES have an exponential dependence on temperature with a $Q_{10}$ of 2.4 taken from Lomas et al. [11] while those in SNP_PERU do not (corresponding to a $Q_{10}$ of 1).

An additional difference between the N_BUR_DOM_CHES (ChesROMS_ECB) and SNP (BioRedoxCNPS) codes is the parameterization of penetrating photosynthetically active radiation (PAR). In N_BUR_DOM_CHES, PAR is attenuated by water, suspended sediments and implicitly by colored dissolved organic materials (via a dependence on salinity) but not by chlorophyll. In SNP_PERU it is attenuated by water and chlorophyll alone. The vertical attenuation of PAR is described by the equation

$$\frac{\partial}{\partial z} PAR = k_{PAR} * PAR \quad (6)$$

where

$$k_{PAR} = 0.04 + 0.024 * Chl \quad (7)$$

Where $Chl$ is the concentration of chlorophyll in mg $m^{-3}$.

*SNP_CHES*

With the exception of temperature dependencies for grazing and remineralization, the code in SNP_CHES is the same as in SNP_PERU. However, in any equations which are also in common with N_BUR_DOM_CHES, all common parameters were set to the values in N_BUR_DOM_CHES. We also adopted the temperature dependences from the N_BUR_DOM_CHES simulation.

*N_BUR_DOM_PERU*

In parallel, we ran N_BUR_DOM_PERU by replacing common parameters in the N_BUR_DOM_CHES code with PERU parameters, including setting $Q_{10}$ to 1 for grazing and remineralization. Thus, comparing SNP_PERU (original BioRedoxCNPS) to SNP_CHES (BioRedoxCNPS with parameters from ChesROMS_ECB) or N_BUR_DOM_CHES (original ChesROMS_ECB) to N_BUR_DOM_PERU (ChesROMS_ECB with parameters from BioRedoxCNPS, see Table 1 in the companion manuscript for list of parameters that differ) helps to

**Table 2**
Biochemical parameters used in SNP_BUR_DOM_CHES.

| Parameter | SNP_BUR_DOM_CHES | Unit |
|---|---|---|
| half-saturation concentration of $O_2$ in oxic mineralization | 0.3 | mmol $O_2$ $m^{-3}$ |
| half-saturation concentration of $NO_3$ in nitrate reduction | 15 | mmol N $m^{-3}$ |
| half-saturation concentration of $NO_2$ in denitrification | 30 | mmol N $m^{-3}$ |
| Threshold value below which nitrite does not participate in denitrification | 2 | mol N $m^{-3}$ |
| half-saturation concentration of $O_2$ inhibition in nitrate reduction and denitrification | 1 | mmol $O_2$ $m^{-3}$ |
| half-saturation concentration of $O_2$ inhibition in sulfate reduction | 0.1 | mmol $O_2$ $m^{-3}$ |
| half-saturation concentration of $NO_3$ inhibition in sulfate reduction | 4 | mmol N $m^{-3}$ |
| constant rate of sulfide oxidation by $NO_3$ | 0.93 | $d^{-1}$ |
| constant rate of sulfide oxidation by $NO_2$ | 0.33 | $d^{-1}$ |
| constant rate of sulfide oxidation by $O_2$ | 0.93 | $d^{-1}$ |
| half-saturation concentration of $O_2$ in sulfide oxidation | 1 | mmol $O_2$ $m^{-3}$ |
| half-saturation concentration of $NO_3$ in sulfide oxidation | 2.9 | mmol N $m^{-3}$ |
| half-saturation concentration of $NO_2$ in sulfide oxidation | 6 | mmol N $m^{-3}$ |
| half-saturation concentration of $O_2$ inhibition in sulfide oxidation | 0.1 | mmol $O_2$ $m^{-3}$ |
| constant rate of anammox rate | 0.07 | $d^{-1}$ (mmol N $m^{-3)\text{-}1}$ |
| maximum rate of aerobic ammonium oxidation | 0.05 | $d^{-1}$ |
| maximum rate of aerobic nitrite oxidation | 0.005 | $d^{-1}$ |
| half-saturation concentration of $O_2$ in nitrification | 1 | mmol N $m^{-3}$ |
| radiation inhibition threshold of ammonium to nitrite oxidation | 0.0095 | W $m^{-2}$ |
| radiation inhibition threshold of nitrite to nitrate oxidation | 0.0364 | W $m^{-2}$ |
| light intensity at which inhibition is half-saturated for ammonium to nitrite oxidation | 0.036 | W $m^{-2}$ |
| light intensity at which inhibition is half-saturated for nitrite to nitrate oxidation | 0.074 | W $m^{-2}$ |
| Small detritus remineralization rate N-fraction | 0.03 | $d^{-1}$ |
| Small detritus remineralization rate C-fraction | 0.03 | $d^{-1}$ |
| Large detritus remineralization rate N-fraction | 0.01 | $d^{-1}$ |
| Large detritus remineralization rate C-fraction | 0.01 | $d^{-1}$ |
| Q_10 | 2.4 | Null |
| phytoplankton growth rate at 0°C | 0.69 | $d^{-1}$ |
| chlorophyll to phytoplankton N maximum ratio | 0.053 | mgChl $mgC^{-1}$ |
| initial slope of planktonic growth to light curve | 0.125 | (W $m^{-2})^{-1}$ $d^{-1}$ |
| half-saturation concentration for uptake of $NO_3$ by phytoplankton | 0.5 | mmol N $m^{-3}$ |
| half-saturation concentration for uptake of $NH_4$ by phytoplankton | 0.5 | mmol N $m^{-3}$ |
| stoichiometry of P to N in phytoplankton and zooplankton | 1/16 | dimensionless |
| Stoichiometry of $O_2$ production/consumption to $NO_3$ uptake/remineralization | 8.625 | dimensionless |
| Stoichiometry of $O_2$ production/consumption to $NH_4$ uptake/remineralization | 6.625 | dimensionless |
| half-saturation concentration for uptake of $PO_4$ by phytoplankton ($kNO_3$ /16) | 0.03125 | mmol P $m^{-3}$ |
| excretion rate due to basal metabolism | 0.1 | $d^{-1}$ |
| excretion rate due to phytoplankton assimilation | 0.1 | $d^{-1}$ |
| assimilation efficiency | 0.75 | dimensionless |
| maximum phytoplankton grazing rate | 0.6 | (mmol N $m^{-3})^{-1}$ $d^{-1}$ |
| phytoplankton mortality | 0.15 | $d^{-1}$ |
| zooplankton mortality | 0.025 | $d^{-1}$ |
| half saturation of phytoplankton ingestion | 2 | (mmol N $m^{-3})^{-2}$ |
| aggregation parameter | 0.005 | $d^{-1}$ |
| sinking velocity of phytoplankton | 0.1 | m $d^{-1}$ |
| sinking velocity of small detritus | 0.1 | m $d^{-1}$ |
| sinking velocity of large detritus | 5 | m $d^{-1}$ |

distinguish the differences that can be attributed to biological parameters (e.g. phytoplankton growth rate) within identical pathways from the differences caused by changing the biogeochemical pathways themselves (e.g. adding anammox).

*SNP_BUR_DOM_PERU*

Since the biological model from al Azhar et al. [2] was developed for an open-ocean/coastal upwelling system rather than an estuary with strong forcing from riverine runoff and significant rates of organic matter burial, we modified the SNP code by adding the resuspension and burial code that was used in ChesROMS_ECB. We also added dissolved organic matter cycling, extending the ECB code which simulated DON and dissolved organic carbon (DOC) to include dissolved organic phosphorus (DOP). Including burial without DOM cycling resulted in an excessive fraction of the nutrients delivered to the model being buried in the river mouths. We denote this merged code as SNP_BUR_DOM, and we denote the simulation made with this new code as SNP_BUR_DOM_PERU when biological constants in common with SNP_PERU are set to those in the latter model.

*SNP_BUR_DOM_CHES*

For the simulation SNP_BUR_DOM_CHES, the code is identical to that of SNP_BUR_DOM_PERU. However, in the equations which are identical to those in N_BUR_DOM_CHES, all parameters are set to the values in the latter simulation. The full set of parameters used in this model is listed in Table 2.

*Pairing simulations to isolate sources of the differences between SNP_PERU and N_BUR_DOM_CHES*

With our six simulations, we can isolate which differences between SNP_PERU and N_BUR_DOM_CHES contribute to the different simulated results. Differences between SNP_PERU and SNP_CHES or N_BUR_DOM_PERU and N_BUR_DOM_CHES are due to differences in parameters common to both simulations. Differences between SNP_BUR_DOM_PERU and SNP_PERU (or SNP_BUR_DOM_CHES and SNP_CHES) are purely due to the inclusion of DOM and burial/resuspension of organic matter. Differences between SNP_BUR_DOM_PERU and N_BUR_DOM_PERU (or SNP_BUR_DOM_CHES and N_BUR_DOM_CHES) are due to differences in whether we include sulfur and phosphorus cycling, or to differences in the optical scheme used to parameterize the penetration of shortwave radiation.

*Developing a new configuration based on SNP_BUR_DOM_CHES–Sensitivity studies and final configuration*

As shown below, SNP_BUR_DOM_CHES produces a simulation that improves nitrate and ammonium relative to N_BUR_DOM_CHES with the new sulfur pathways, but only at the cost of reducing the fidelity of the oxygen simulation and creating a high bias for nitrite. Starting with this simulation we then show that we can improve individual fields by:

1. Changing the optics to include implicit CDOM and explicit sediment absorption: In this case, we change the optics in SNP_BUR_DOM_CHES to the formulation in N_BUR_DOM_CHES which implicitly relates the diffuse attenuation coefficient to refractory DOC delivered down rivers.

$$k_{PAR} = \max(1.4 + 0.063 * TSS - 0.057 * S, 0.6) \tag{8}$$

where TSS represents total suspended solids. Note that as S becomes very small, the attenuation becomes very large.

2. Making nitrification and denitrification easier: In this case, we decrease half-saturation concentration of $NO_2$ in denitrification from 30 mmol N $m^{-3}$ to 1 mmol N $m^{-3}$ and increase nitrification rate constant governing the transformation of $NO_2$ to $NO_3$ from 0.005 $day^{-1}$ to 0.05 $day^{-1}$. We also remove 2 mmol/$m^3$ threshold for nitrite to participate in denitrification.
3. Increasing the stoichiometric ratio between N and O in organic matter: In this case, we increase oxygen:nitrate from 8.625 to 9.625 and oxygen:ammonium from 6.625 to 7.625, for reasons justified below (See section “motivating the sensitivity cases: $O_2$:N Stoichiometry").

In the companion paper, we showed some of the impacts of these three changes on nitrogen partitioning (Fig. 9) and model fidelity for oxygen, ammonium and nitrate at CB3.3 (Table 6). In this manuscript we expand the evaluation to other sites, consider nitrite biases and also evaluate the impacts of making all three changes simultaneously.

*Evaluation of model configurations*

At station CB3.3, significant differences between simulations of oxygen, ammonium and nitrate using the two published codes are found (right-hand column of Fig. 4 in companion paper). As illustrated in Fig. 1, we now break down the differences between the original models into the three categories described in the companion Ocean Modelling manuscript [10] demonstrating that it does not matter (at least qualitatively) in which order changes are made.

*Impact of using the PERU parameter set vs CHES parameter set in the two BGC codes*

While there are many differences between the biogeochemical cycles in the two published codes, parameters such as growth rates and sinking speeds of detritus that are found in both codes also differ. These common parameters would be expected to have effects on our model results. To quantify this effect, we compare two pairs of models: SNP_PERU minus SNP_CHES (left column of Fig. 2) and N_BUR_DOM_PERU minus N_BUR_DOM_CHES (right column of Fig. 2). This comparison isolates the differences contributed by changing common parameters from their values in Da et al. [5] to the values in Hantsoo et al. [8] and vice versa.

Switching parameters from CHES values to PERU values does not explain the differences in the third column in Fig. 4 of companion paper; in fact, the changes seen have the opposite sign. Qualitatively similar changes are seen in the two pairs of simulations. Oxygen becomes higher from near the bottom to around 8 m in depth. Nitrate gets higher while ammonium becomes lower. SNP_PERU minus SNP_CHES shows more extreme change for oxygen and ammonium with more moderate change for nitrate compared to N_BUR_DOM_PERU minus N_BUR_DOM_CHES. SNP_PERU has much more oxygen than SNP_CHES from late January to mid-April and late November to end of December from near the bottom to 10 m in depth, with relative increases of up to 200 mmol $O_2/m^3$. SNP_CHES extends the hypoxic zone at CB3.3C through much of the year. In both pairs, using PERU parameters leads to a lower oxygen concentration near the surface, especially during the summer months. From late January to mid-April as well as in December, nitrate in SNP_PERU is up to 25 mmol N/$m^3$ higher than SNP_CHES. This can be explained in terms of the higher levels of oxygen in SNP_PERU reducing denitrification rates, allowing nitrate to persist longer for the PERU parameters relative to the CHES parameters. Nitrate in N_BUR_DOM_PERU is always higher than N_BUR_DOM_CHES, especially from early June to mid-July, by up to 50 mmol N/$m^3$. For ammonium, SNP_PERU is consistently up to 20 mmol N/m3 lower than SNP_CHES from near the bottom to a depth of 10 m. N_BUR_DOM_PERU is also lower than N_BUR_DOM_CHES, but the largest differences occur only in June. The middle column of Fig. 6 in

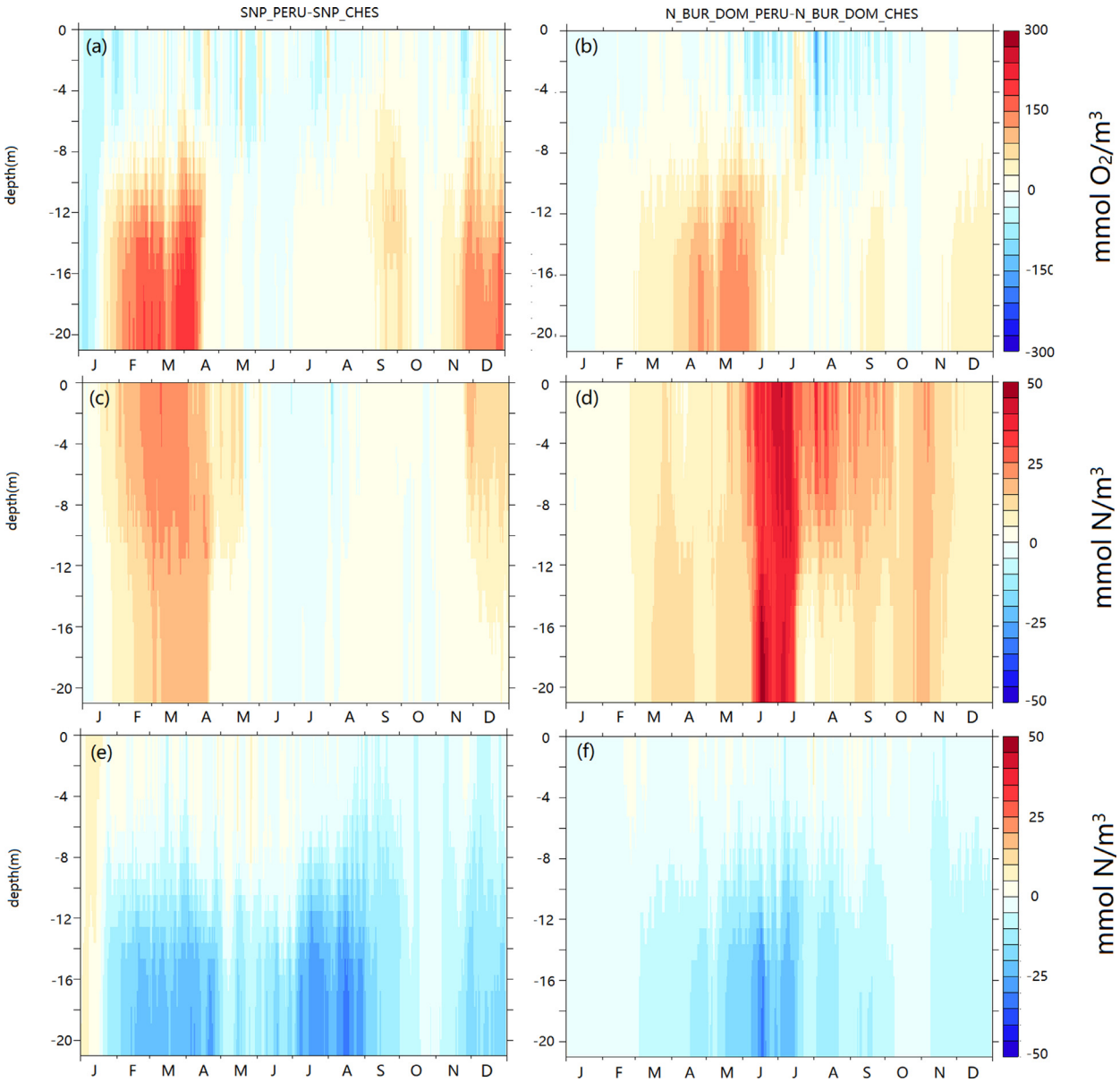


**Fig. 2.** Evaluation of the consistency of the effect of changing common parameters. Modeled oxygen (a, b), nitrate (c, d) and ammonium (e, f) for SNP_PERU minus SNP_CHES (left column, a, c and e) and N_BUR_DOM_PERU minus N_BUR_DOM_CHES (right column, b, d and f) at coincident times and locations at the Bay Bridge station (CB3.3C) during 2017.

the companion paper also demonstrates similar changes when transitioning from SNP_BUR_DOM_PERU to SNP_BUR_DOM_CHES. This indicates that the effects of changing common parameters are robust across various model configurations.

*Impact of adding burial and DOM to the SNP code*

Next, we turn to the differences between the simulations induced by adding or removing burial of organic matter and cycling of dissolved organic matter, processes which are not included in the original SNP code of al Azhar et al. [2]. Differences between SNP_CHES versus SNP_BUR_DOM_CHES (Fig. 3 left column) and SNP_PERU versus SNP_BUR_DOM_PERU (right column in Fig. 6 of the companion paper) in oxygen, nitrate and ammonium are shown. We choose to show the impacts of *removing* burial and DOM cycling so as to make it easier to visually attribute the differences between the original models to different sources.

For both pairs of simulations, removing dissolved organic matter and burial processes generally more than balances the oxygen and ammonium changes caused by changes in common parameters and thus plays a leading role in explaining the differences between

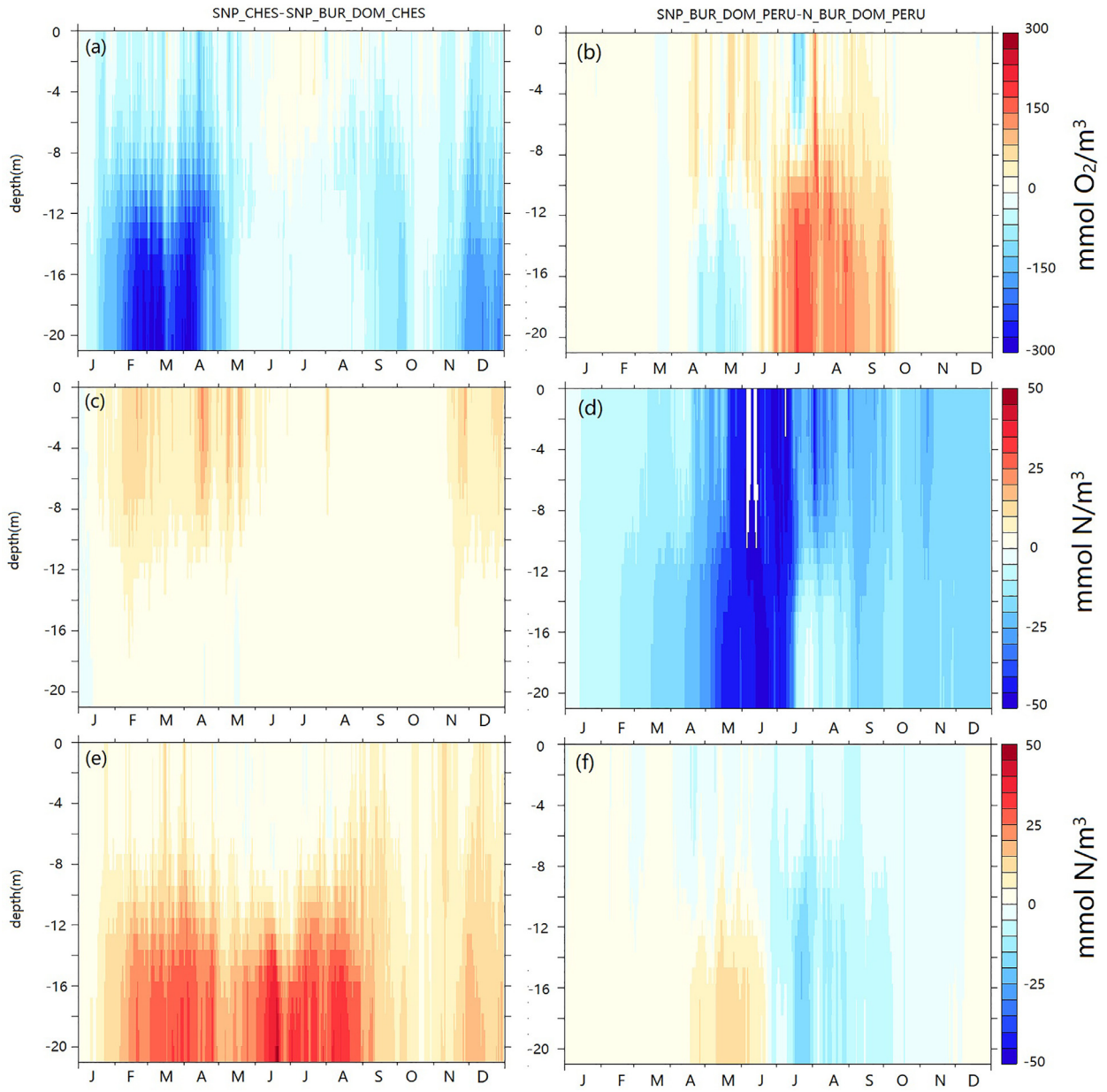


**Fig. 3.** Evaluation of the consistency of the effect of removing DOM and burial and the consistency of the effect of changing pathways and optics. Modeled oxygen (a, b), nitrate (c, d) and ammonium (e, f) for SNP_CHES minus SNP_BUR_DOM_CHES (left column, a, c and e) and SNP_BUR_DOM_PERU minus N_BUR_DOM_PERU (right column, b, d and f) at coincident times and locations at the Bay Bridge station (CB3.3C) during 2017.

the original models. Both pairs of simulations show decreases in oxygen and increases in ammonium concentrations from the bottom to around 8 m in depth, although the time period during which the decrease is seen is different in the two comparisons.

Oxygen in SNP_CHES is lower than SNP_BUR_DOM_CHES for most of the year, with significant differences appearing from mid-January to early May and late November to late December. During the summer months, oxygen in SNP_CHES is slightly higher than SNP_BUR_DOM_CHES near the surface. Larger difference values for SNP_PERU versus SNP_BUR_DOM_PERU are found from early April to early October. For the most part, surface oxygen concentrations during summertime in SNP_PERU are slightly higher than SNP_BUR_DOM_PERU. SNP_CHES shows much higher values of ammonium than SNP_BUR_DOM_CHES from mid-February to late August, while in SNP_PERU the higher values appear from late May to mid-August. For nitrate, SNP_CHES is almost always higher than SNP_BUR_DOM_CHES with largest differences appearing near the surface from late January to mid-May and mid-November to late December. However, from late April to mid-May nitrate in SNP_PERU is slightly lower than SNP_BUR_DOM_PERU. The differences

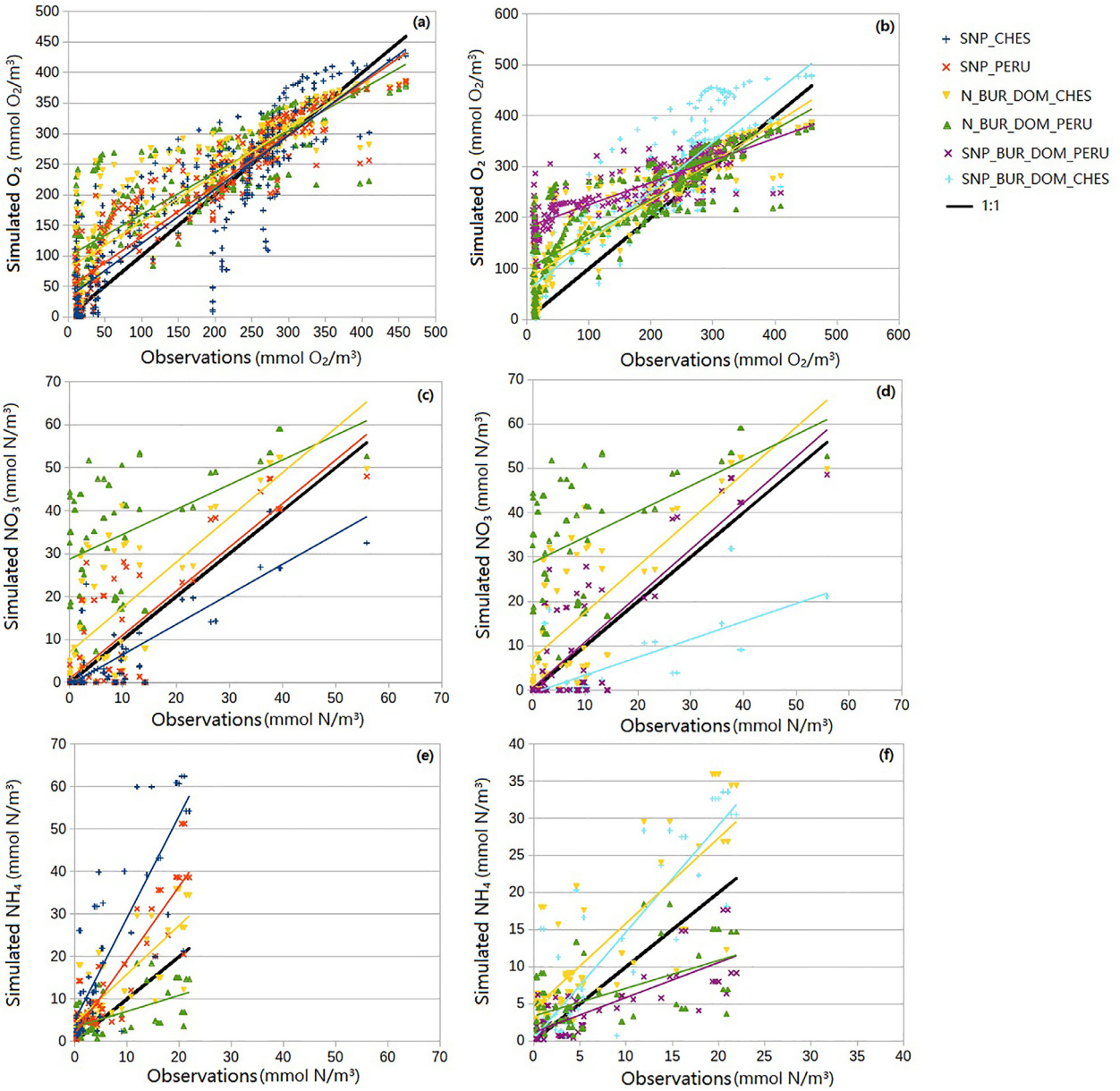


**Fig. 4.** Simulated versus observed oxygen (mmol $O_2/m^3$) (a,b), nitrate (mmol $N/m^3$) (c, d) and ammonium (mmol $N/m^3$) (e, f) at coincident times and locations from SNP_CHES (blue), SNP_PERU (orange), N_BUR_DOM_CHES (yellow), N_BUR_DOM_PERU (green), SNP_BUR_DOM_PERU (purple) and SNP_BUR_DOM_CHES (light blue). Left column shows cases that can be used to compare CHES (dark blue cross, yellow triangle) and corresponding PERU (orange cross, green triangle) parameter sets. Right column shows cases that can be used to evaluate impact of adding new pathways and changing optics (compare light blue with green, purple with yellow). Solid black lines show 1:1 line, colored lines show linear trend. Note that the scales differ between (a) and (b), (e) and (f) in order to make the differences between simulations more visible.

in nitrate are much smaller than the increases resulting from changing common parameters and so do not explain the differences between the original configurations seen in Fig. 4 of our companion paper.

*Impact of the effects of nutrient cycling and optics changes between the two BGC codes: Coupled sulfur, nitrogen and phosphate cycling*

We now turn to the differences induced by adding the pathways for sulfur and phosphorus cycling, explicitly modeling nitrite and anammox and changing the optics in al Azhar et al. [2] but not changing burial or dissolved organic matter cycling. Differences between SNP_BUR_DOM_PERU versus N_BUR_DOM_PERU simulations of oxygen, nitrate and ammonium are shown in right column

**Table 3**
Error metrics for the model suite compared with observations. A perfect model would have $R^2$=1 and bias=0. Values of $R^2$<0 are associated with large biases, which result in the error variance being larger than the sample variance. Because the biases of nitrite dominate the $R^2$ we only report biases here.

| | $R^2$/bias for $O_2$ | $R^2$/bias for $NH_4$ | $R^2$/bias for $NO_3$ | bias for $NO_2$ |
|---|---|---|---|---|
| N_BUR_DOM_CHES | 0.72/36.44 | -0.32/5.32 | -0.29/7.49 | NA |
| N_BUR_DOM_PERU | 0.59/41.61 | 0.27/-0.69 | -4.77/24.94 | NA |
| SNP_CHES | 0.75/10.66 | -8.17/14.14 | 0.62/-3.19 | 5.16 |
| SNP_PERU | 0.85/17.39 | -1.13/6.58 | 0.46/1.08 | 10.20 |
| SNP_BUR_DOM_CHES | 0.59/51.23 | -0.03/3.14 | 0.20/-6.02 | 4.33 |
| SNP_BUR_DOM_PERU | 0.19/78.95 | 0.46/-2.28 | 0.49/0.86 | 8.48 |

of Fig. 3. Differences between SNP_BUR_DOM_CHES versus N_BUR_DOM_CHES can be seen in left column of Fig. 6 in our companion paper.

Adding more complex nutrient cycling and changing the optics produces large decreases in nitrate—explaining why we see decreases in this field in Fig. 4 of our companion paper, but produces smaller changes in oxygen and ammonium. Similar changes for the two pairs of simulations are seen in nitrate and ammonium. Relative to the original ChesROMS_ECB code, the SNP code decreases nitrate concentration: large decreases (up to 50 mmol N/$m^3$) appear from early May to mid-July for SNP_BUR_DOM_PERU minus N_BUR_DOM_PERU, and from late January to early June for SNP_BUR_DOM_CHES minus N_BUR_DOM_CHES. The changes in pathways thus appear to dominate the differences in nitrate seen in the two published models.

For ammonium, SNP_BUR_DOM_PERU predicts values up to 15 mmol N/$m^3$ higher than N_BUR_DOM_PERU from early May to early June from bottom to 14 m in depth but up to 30 mmol N/$m^3$ lower in July. Similar changes can be observed in SNP_BUR_DOM_CHES minus N_BUR_DOM_CHES but the range is less extreme. The changes in nutrient cycling and optics are important for determining the timing of the differences in ammonium seen in Fig. 4 of our companion paper but are not the dominant drivers of these differences.

In contrast to nitrate and ammonium, the differences in oxygen induced by adding nutrient cycling and changing the optics depend more on the base simulation. From the bottom to 12 m in depth, oxygen in SNP_BUR_DOM_PERU is lower than N_BUR_DOM_PERU from late April to early June, while from early June to early October, oxygen in SNP_BUR_DOM_PERU becomes higher than N_BUR_DOM_PERU. During the same period and at the same location, SNP_BUR_DOM_CHES and N_BUR_DOM_CHES only exhibit minor differences. During the summer months near the surface, SNP_BUR_DOM_PERU is mostly higher than N_BUR_DOM_PERU while SNP_BUR_DOM_CHES is mostly lower than N_BUR_DOM_CHES. Overall, these differences are smaller than those associated with the previous pairs of experiments.

*Evaluating the realism of the model simulations-Is there a best simulation?*

Evaluation of simulations for oxygen, nitrate and ammonium from the two published models can be found in our companion paper in section 3.1. Here we also list the $R^2$ and bias of nitrite and metrics from SNP_BUR_DOM_CHES and SNP_BUR_DOM_PERU for a more complete comparison which serves as the basis for constructing the best model. All of the SNP simulations show an improvement for the simulation of nitrate at CB3.3.

However, examining the $R^2$ and biases for oxygen, nitrate and ammonium across the models listed in Table 3 demonstrates that the "best" model is not the same for each variable. Large biases play a significant role in decreasing $R^2$: SNP_CHES has a high ammonium bias of 14.14 with an $R^2$ of -8.17 while N_BUR_DOM_PERU has a high nitrate bias of 24.94 with an $R^2$ of -4.77. In terms of $R^2$ averaged across the three variables and also low biases for nitrogen variables, SNP_BUR_DOM_PERU produces the best simulation at CB3.3C. However, the results come at the cost of a degradation of the simulation of oxygen. A tradeoff can be seen between nitrate/ammonium and oxygen simulations among the six simulations. We will return to the implications of this result in the following section.

By examining scatter plots comparing observations (horizontal axis) to the modeled values (vertical axis) across these sets of simulations (Fig. 4), we can see more details about which mismatches contribute to the $R^2$ differences, and whether this remains consistent across simulations.

The top row shows the model-data mismatch for oxygen. We can look at the impact of changing parameter sets by comparing SNP_CHES (yellow, Fig. 4a) with SNP_PERU (orange, Fig. 4a), N_BUR_DOM_CHES (blue, Fig. 4a) with N_BUR_DOM_PERU (green, Fig. 4a) and SNP_BUR_DOM_CHES (light blue, Fig. 4b) with SNP_BUR_DOM_PERU (purple, Fig. 4b). All the models generally overpredict oxygen with the worst mismatch in the 50-200 mmol $O_2$/$m^3$ range. Switching from PERU to CHES parameters reduces this mismatch across all three pairs, with the trend lines for SNP_PERU, N_BUR_DOM_PERU and SNP_BUR_DOM_PERU (orange, blue, purple) lying above those for SNP_CHES, N_BUR_DOM_CHES and SNP_BUR_DOM_CHES (yellow, green, light blue). However, at higher values of oxygen the trends reverse. Which parameter set is used modulates the impact of adding new pathways (illustrated in Fig. 4b). SNP_BUR_DOM_PERU has more oxygen than N_BUR_DOM_PERU at the low end of the range but less at the high end, while the reverse is true for SNP_BUR_DOM_CHES with respect to N_BUR_DOM_CHES. Adding dissolved organic matter and burial processes slightly increases the overestimation of oxygen relative to observations in the 50-200 mmol $O_2$/$m^3$ range.

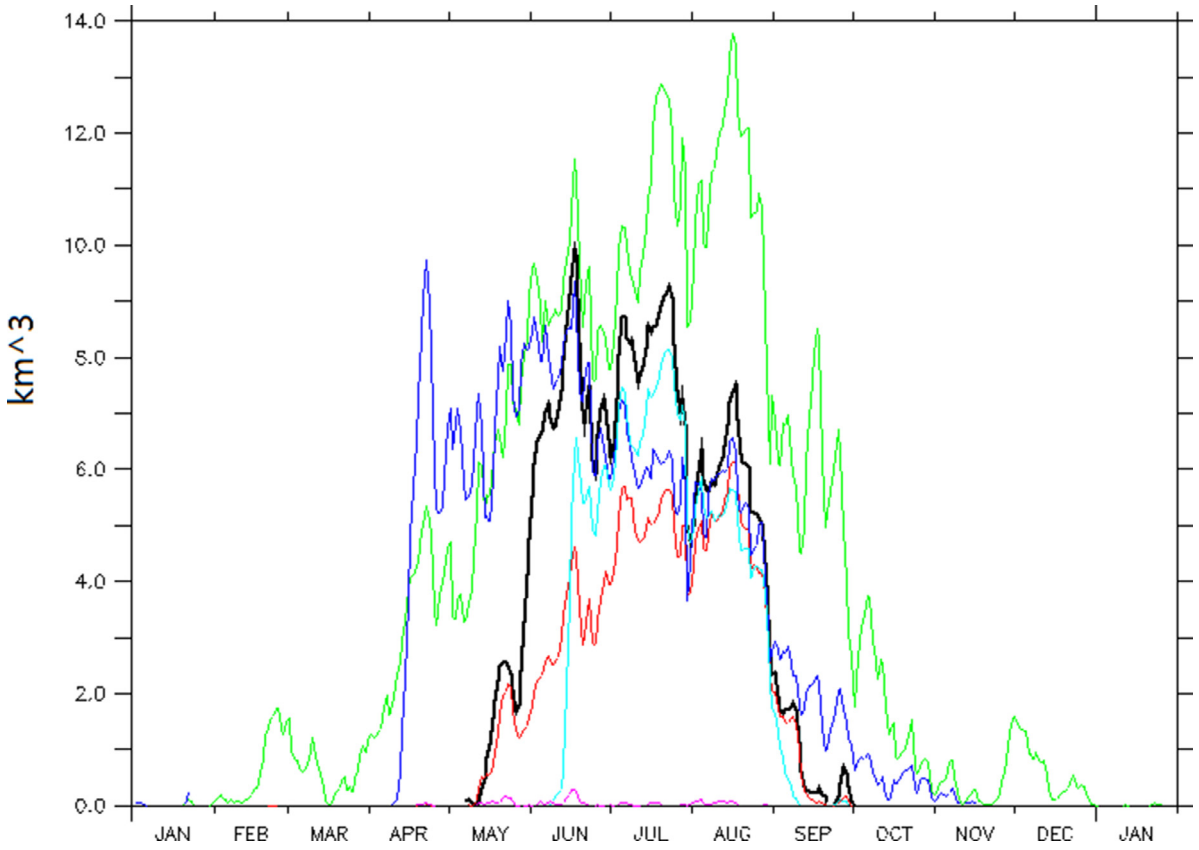


**Fig. 5.** Hypoxic volume for six runs: N_BUR_DOM_CHES (VIMS hindcast, black), SNP_CHES (green), SNP_BUR_DOM_CHES (red), SNP_PERU (dark blue), N_BUR_DOM_PERU (light blue) and SNP_BUR_DOM_PERU (purple).

For nitrate (middle row) and ammonium (bottom row) the changes are clearer and more consistent across the range of observed values. Holding other factors constant, the PERU parameter set lies above the corresponding CHES parameter set for almost all nitrate samples and below it for almost all ammonium samples. However, for nitrate the ranges over which the changes occur are not the same. N_BUR_DOM_PERU largely increases nitrate at the low end of the range relative to N_BUR_DOM_CHES while the SNP_PERU/SNP_BUR_DOM_PERU simulations see the increase more at the upper end of the range relative to SNP_CHES/SNP_BUR_DOM_CHES. Adding dissolved organic matter and burial processes lowers both the nitrate and ammonium concentrations. Adding pathways generally lowers nitrate (Fig. 4d) and has a relatively small impact on ammonium (Fig. 4f).

*Hypoxic volume time series*

An alternative diagnostic of model accuracy of interest to policy makers is the total volume of hypoxic waters (oxygen concentrations less than 62.5 mmol/$m^3$). As previously noted, N_CHES_BUR_DOM has been used as to hindcast hypoxia within the Bay and so large deviations from what it predicts (black line Fig. 5) are suspect. As shown in Fig. 5, SNP_CHES (green line Fig. 5) produces far too much hypoxia and SNP_BUR_DOM_PERU (purple line, Fig. 5) produces far too little. SNP_PERU (dark blue line, Fig. 5) produces too much hypoxia early in the spring and the first appearance of hypoxia in N_BUR_DOM_PERU (light blue Line, Fig. 5) is too late in the summer. SNP_BUR_DOM_CHES has a simulation similar to VIMS hindcast in terms of when hypoxia appears and disappears, but the magnitude of peak hypoxic volume is significantly smaller.

*$R^2$ results for other sites*

Extending the model simulations to two other sites in Chesapeake Bay (CB2.2 at the northern end of the hypoxic zone, Table 4 and CB5.3 at the southern end of the hypoxic zone, Table 5) further shows the necessity of constructing a better model that can skillfully simulate biogeochemical fields throughout the Bay. N_BUR_DOM_CHES does not do a good job at predicting the annual cycle of many fields at these sites, specifically nitrate and ammonium at CB5.3 and all three fields at CB2.2. While other model configurations can improve the simulation of individual species at individual sites, no one simulation produces an improvement for oxygen, ammonium and nitrate at all sites, and in general improving the simulation of ammonium makes the simulation of oxygen worse and vice versa.

**Table 4**
Error metrics for the model suite compared with observations at CB2.2.

| | N_BUR_DOM_CHES | SNP_PERU | SNP_CHES | N_BUR_DOM_PERU | SNP_BUR_DOM_CHES | SNP_BUR_DOM_PERU |
|---|---|---|---|---|---|---|
| Oxygen | 0.28 | 0.73 | -0.17 | -0.23 | -2.47 | -1.41 |
| Nitrate | -0.03 | 0.11 | 0.02 | -22.66 | -3.82 | -7.57 |
| Ammonium | -1.49 | -6.99 | -5.72 | 0.01 | -0.27 | -0.36 |

**Table 5**
Error metrics for the model suite compared with observations at CB5.3.

| | N_BUR_DOM_CHES | SNP_PERU | SNP_CHES | N_BUR_DOM_PERU | SNP_BUR_DOM_CHES | SNP_BUR_DOM_PERU |
|---|---|---|---|---|---|---|
| Oxygen | 0.82 | 0.47 | 0.78 | 0.50 | 0.23 | -0.03 |
| Nitrate | -7.29 | -4.54 | -0.43 | 0.45 | -0.59 | -0.20 |
| Ammonium | -9.48 | -9.37 | -9.13 | 0.72 | 0.27 | -0.46 |

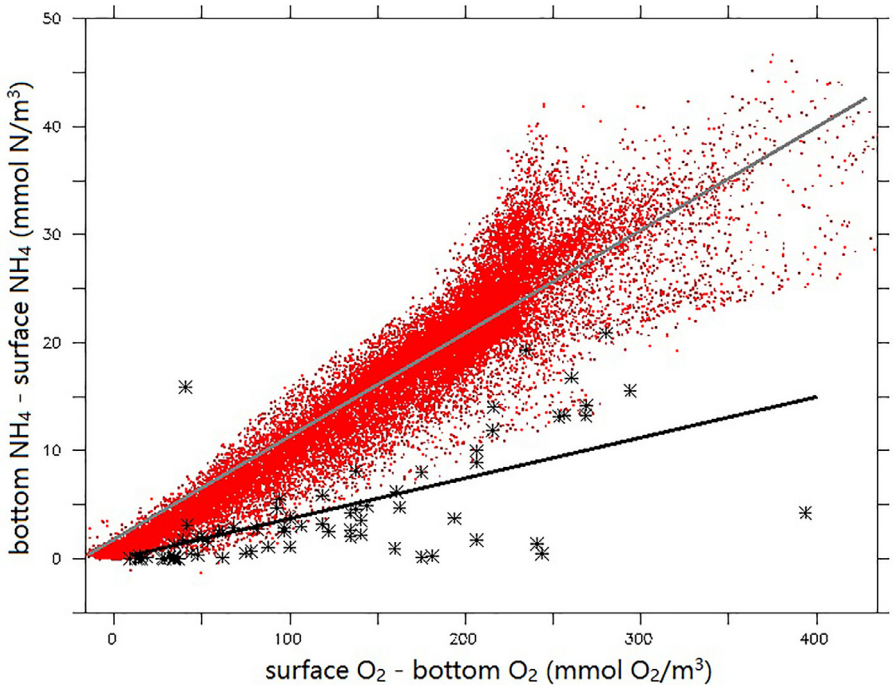


**Fig. 6.** Modeled surface oxygen minus bottom oxygen (mmol $O_2/m^3$) vs bottom $NH_4$ minus surface $NH_4$ (mmol $N/m^3$) from SNP_BUR_DOM_CHES (red dots) vs observations (black symbols) from 2017. The grey line shows the trend for the simulation while the black line shows the trend for the observations.

*Motivating the sensitivity cases*

$O_2$:N Stoichiometry: One potential reason for the tradeoff between our simulations of ammonium and oxygen is stoichiometry. As shown in Fig. 6, during the summertime, the vertical gradient of oxygen tightly tracks the ammonium vertical gradient with a slope of 0.08 in SNP_BUR_DOM_CHES. However, when we look at observations, we see a shallower relationship between oxygen gradient and ammonium gradient, with a slope of 0.04 (Fig. 6 solid black line). This suggests a systematic problem in how our models are constructed. Given that the slope (0.08) between gradient of oxygen and gradient of ammonium of our simulation is around two times higher than the corresponding slope (0.04) of observations, this suggests that nitrogen should be more efficient at removing oxygen, in other words the $O_2$:N stoichiometric ratio should be higher than in the previously published models. We make a relatively small change in our sensitivity study, increasing oxygen:nitrate from 8.625 to 9.625 and oxygen:ammonium from 6.625 to 7.625.

Optics: The different representation of light attenuation in SNP_BUR_DOM_CHES versus N_BUR_DOM_CHES also has a large effect in model performance. As noted in the companion paper, in the first half of 2017 SNP_BUR_DOM_CHES has much more primary productivity (30.3 Gmol N vs. 6.7 Gmol N) and burial of nitrogen (2.7 Gmol N vs. 1.35 Gmol N) than N_CHES_BUR_DOM. Analysis of

**Table 6**
Error metrics at CB3.3 for the sensitivity cases compared with observations. A perfect model would have $R^2$=1 and bias=0. Values of $R^2$<0 are associated with large biases, which result in the error variance being larger than the sample variance. Because biases dominate the error for nitrite we focus on biases here.

| | $R^2$/bias for $O_2$ | $R^2$/bias for $NH_4$ | $R^2$/bias for $NO_3$ | bias for $NO_2$ |
|---|---|---|---|---|
| SNP_BUR_DOM_CHES | 0.59/51.23 | -0.03/3.14 | 0.20/-6.02 | 4.33 |
| Higher $O_2$:N ratio | 0.58/51.23 | -0.15/3.35 | 0.19/-6.03 | 3.96 |
| Add CDOM absorption | 0.73/35.27 | 0.72/1.39 | 0.49/2.49 | 12.71 |
| Make nitrification/denitrification easier | 0.61/50.22 | -1.46/5.36 | 0.20/-5.91 | 0.86 |
| Reference | 0.78/28.15 | 0.33/5.01 | 0.26/4.36 | 3.78 |

**Table 7**
Error metrics for the model suite compared with observations at CB 2.2 and CB5.3.

| $R^2$ of CB2.2 | SNP_BUR_DOM_CHES | Add CDOM | Easier (de)nitrification | Higher ratio | Reference |
|---|---|---|---|---|---|
| Oxygen | -2.47 | 0.40 | -2.30 | -2.89 | 0.39 |
| Nitrate | -3.82 | 0.04 | -1.96 | -1.98 | -1.87 |
| Ammonium | -0.27 | -1.44 | -1.15 | -1.10 | -0.19 |
| $R^2$ of CB5.3 | SNP_BUR_DOM_CHES | Add CDOM | Easier (de)nitrification | Higher ratio | Reference |
| Oxygen | 0.23 | 0.88 | 0.75 | 0.77 | 0.82 |
| Nitrate | -0.59 | -3.12 | -0.38 | -0.37 | -3.93 |
| Ammonium | 0.27 | -2.43 | -1.42 | -1.06 | -5.89 |

why this might be the case showed that SNP_BUR_DOM_CHES had a much deeper penetration of light, more primary productivity at depth and more material hitting the bottom. To evaluate the impact of changing the light attenuation we run a simulation in which the chl-only absorption in the SNP run was replaced by the formulation in Da et al. [5] reported in Eq. 8.

Ease of nitrification/denitrification: As also seen in our companion paper, the SNP runs (including SNP_BUR_DOM_CHES) exhibit a high bias for nitrite. However as previously noted, these runs set minimum thresholds for nitrite to denitrify and had a very slow rate of governing the conversion of nitrite to ammonium. We show the impacts of setting the denitrification thresholds to zero, decreasing half-saturation concentration of $NO_2$ in denitrification from 30 mmol N $m^{-3}$ to 1 mmol N $m^{-3}$ and increasing the rate constant for nitrite to ammonium conversion so that it matches the conversion rate of nitrate to nitrite (0.05 $day^{-1}$). Finally, we developed a new reference simulation that included all three of these changes.

*Combining multiple changes to improve the simulation: simulation of hydrography at CB3.3*

The values for $R^2$ and bias shown in Table 6 demonstrate that our different changes help to improve performance of SNP_BUR_DOM_CHES in different ways. Increasing the stoichiometric ratios drops the nitrite bias while slightly degrading the simulation of oxygen, ammonium and nitrate. Adding CDOM absorption dramatically increases skills for simulating oxygen, nitrate and ammonium, but it gives unrealistic results for nitrite. Making nitrification easier significantly reduces the bias for nitrite, but at the cost of decreasing $R^2$ for oxygen, nitrate and ammonium. Combining all those changes (bottom row) gives us a simulation that produces better joint simulations of oxygen, nitrate and ammonium at CB3.3 (as given by the sum of the three $R^2$ terms) than either N_BUR_DOM_CHES or SNP_PERU (the two published models). Additionally, it does so while reducing the high nitrite bias seen in the SNP models, though nitrite is still overestimated.

Scatter plots (Fig. 7) show that for oxygen, adding CDOM absorption gives best results comparing with observations. SNP_BUR_DOM_CHES along with the two other cases overpredict oxygen. For nitrate, adding CDOM absorption also gives the most similar results to observations while other cases underestimate nitrate. Finally, adding CDOM absorption leads us to somewhat underestimated ammonium, but the resulting simulation is still better compared to other cases.

*Combining multiple changes to improve the simulation: Hypoxic volumes*

Turning to the predicted hypoxic volume for three cases, Fig. 8 shows that adding CDOM absorption increases hypoxia earlier in summer. Making nitrification/denitrification easier or increasing the stoichiometric ratio both increase hypoxia when compared with SNP_BUR_DOM_CHES.

*Combining multiple changes to improve the model: $R^2$ from other sites*

As seen in Table 7, the changes in hydrographic fields seen at CB3.3 translate to some extent to the northern site. We find that the optics changes improve oxygen and nitrate but make ammonium worse at CB2.2. At CB5.3 changing the optics makes oxygen much better but makes nitrite and ammonium worse. Making nitrification and denitrification easier improves all three fields at CB2.2 (in notable contrast to CB3.3, where they all get slightly worse), improves oxygen and nitrate at CB5.3, but makes ammonium worse.

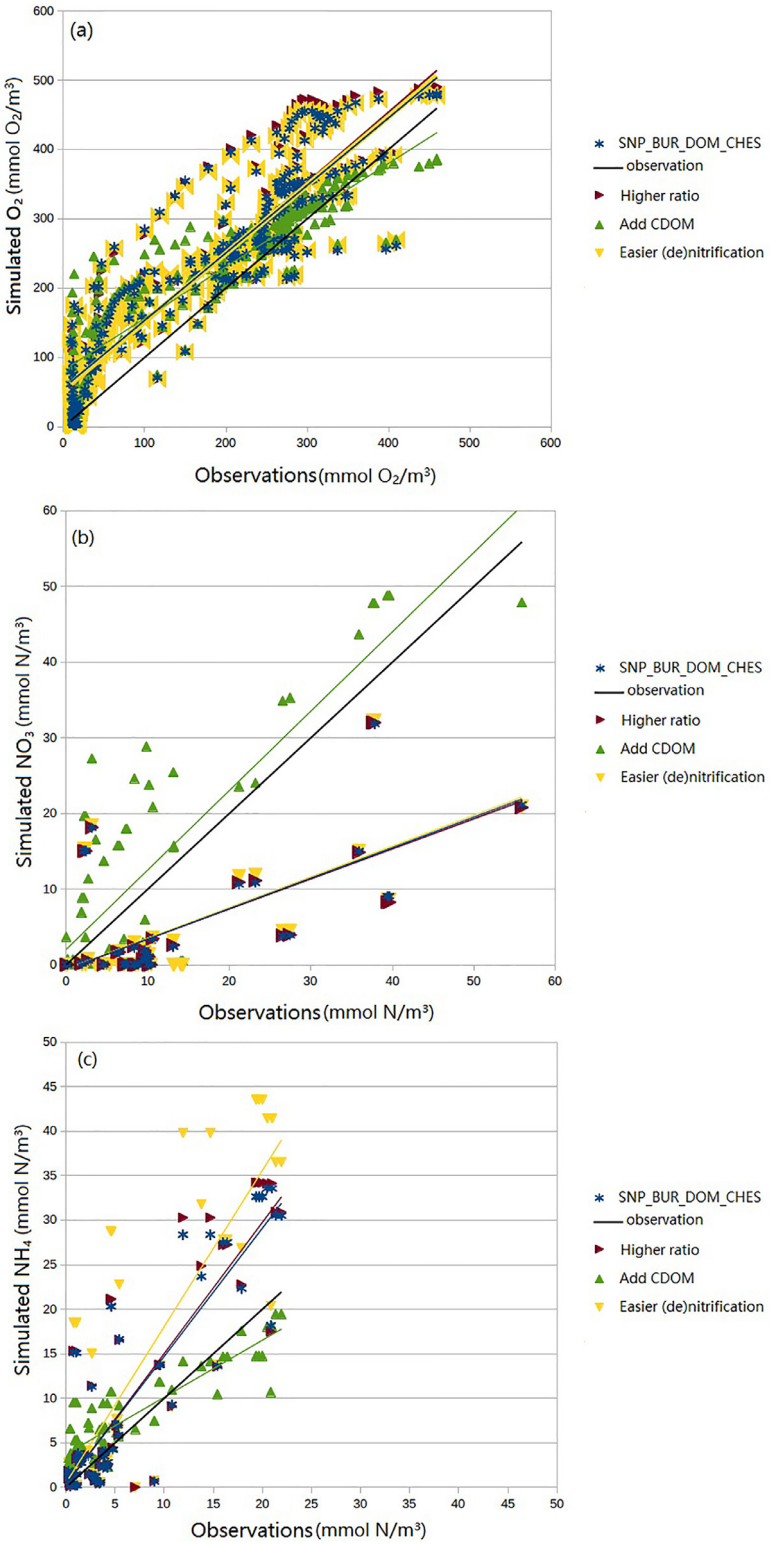


**Fig. 7.** Simulated versus observed (a) oxygen (mmol $O_2/m^3$) (b) nitrate (mmol $N/m^3$) (c) and ammonium (mmol $N/m^3$) at coincident times and locations from SNP_CHES_BUR_DON (blue) and three sensitivity cases, one with increased $O_2$:N stoichiometric ratio (purple triangles), one including CDOM absorption in the optics (green triangle) and one that makes nitrification and denitrification easier (yellow triangle).

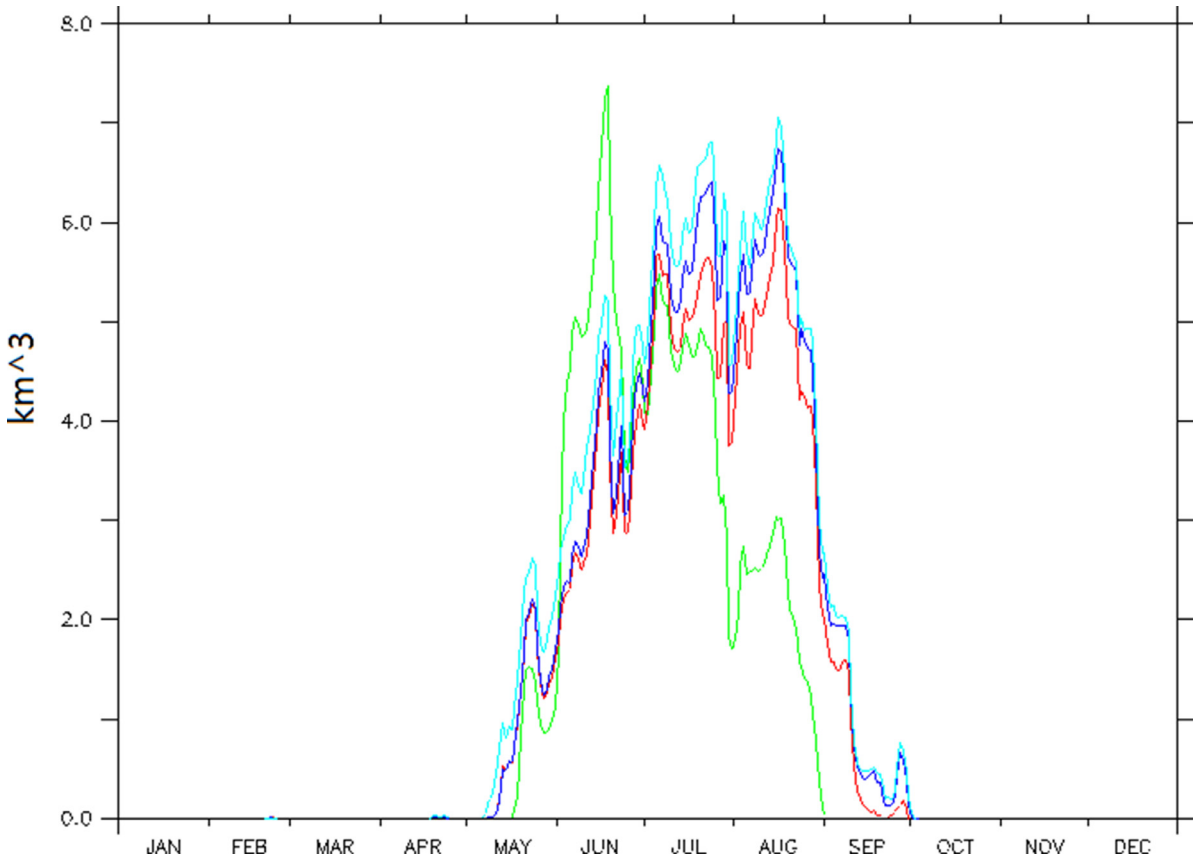


**Fig. 8.** Hypoxic volume for three sensitivity cases: SNP_BUR_DOM_CHES (red), adding CDOM absorption (green), making nitrification/denitrification easier (dark blue), increasing $O_2$:N stoichiometric ratio (light blue).

Increasing the $O_2$:N ratio improves nitrate at CB2.2 but makes ammonium and oxygen worse, and improves oxygen and nitrate at CB5.3 while again making ammonium worse.

*Performance of merged (new reference) model*

While the bulk statistics make it clear that our new reference run does a better job at simulating oxygen, nitrate and ammonium at CB3.3 than the SNP_BUR_DOM_CHES run on which it is based, it is not clear which parts of the spatiotemporal distribution are improved. Scatter plots (Fig. 9) clearly show that the new reference simulation can simulate oxygen, nitrate and ammonium reasonably well. From 0-200 mmol $O_2/m^3$ range, it still slightly overestimates oxygen, but in 200-500 mmol $O_2/m^3$ range, it simulates oxygen levels that are very close to observations. The new reference run overestimates nitrate but to a much smaller degree than SNP_BUR_DOM_CHES underestimates it. Our reference run also slightly overestimates ammonium in 0-5 mmol $N/m^3$ range but simulates it well in 5-25 mmol $N/m^3$ range.

*Hypoxic volume in reference run*

Finally, we turn to hypoxic volume. As shown in Fig. 10, our new reference run gives a very similar simulation of hypoxic volume as in VIMS hindcast (black), much better than SNP_BUR_DOM_CHES (red), which has a lower volume in the summer.

To conclude, our merged model SNP_BUR_DOM_CHES with CDOM absorption, increased stoichiometric $O_2$:N ratio and easier nitrification and denitrification produces a reasonable simulation for oxygen, nitrate, ammonium and hypoxic volume. In most cases it produces lower errors for all three fields relative to the original N_BUR_DOM_CHES model at CB2.2 at the northern edge of the hypoxic zone, CB3.3 in the heart of the hypoxic zone, and CB5.3 at the southern edge of the hypoxic zone though the best simulation is found at CB3.3. The one exception is nitrate at CB2.2, which is overestimated in the reference run at CB2.2. Our new model has a comparable simulation of hypoxia to N_BUR_DOM_CHES, which has been used for hindcasting hypoxia in the Bay. Our new model also has much lower nitrite biases than any of the SNP series of models. While nitrite bias remains a problem, we believe this model can be used as a basis for future work.

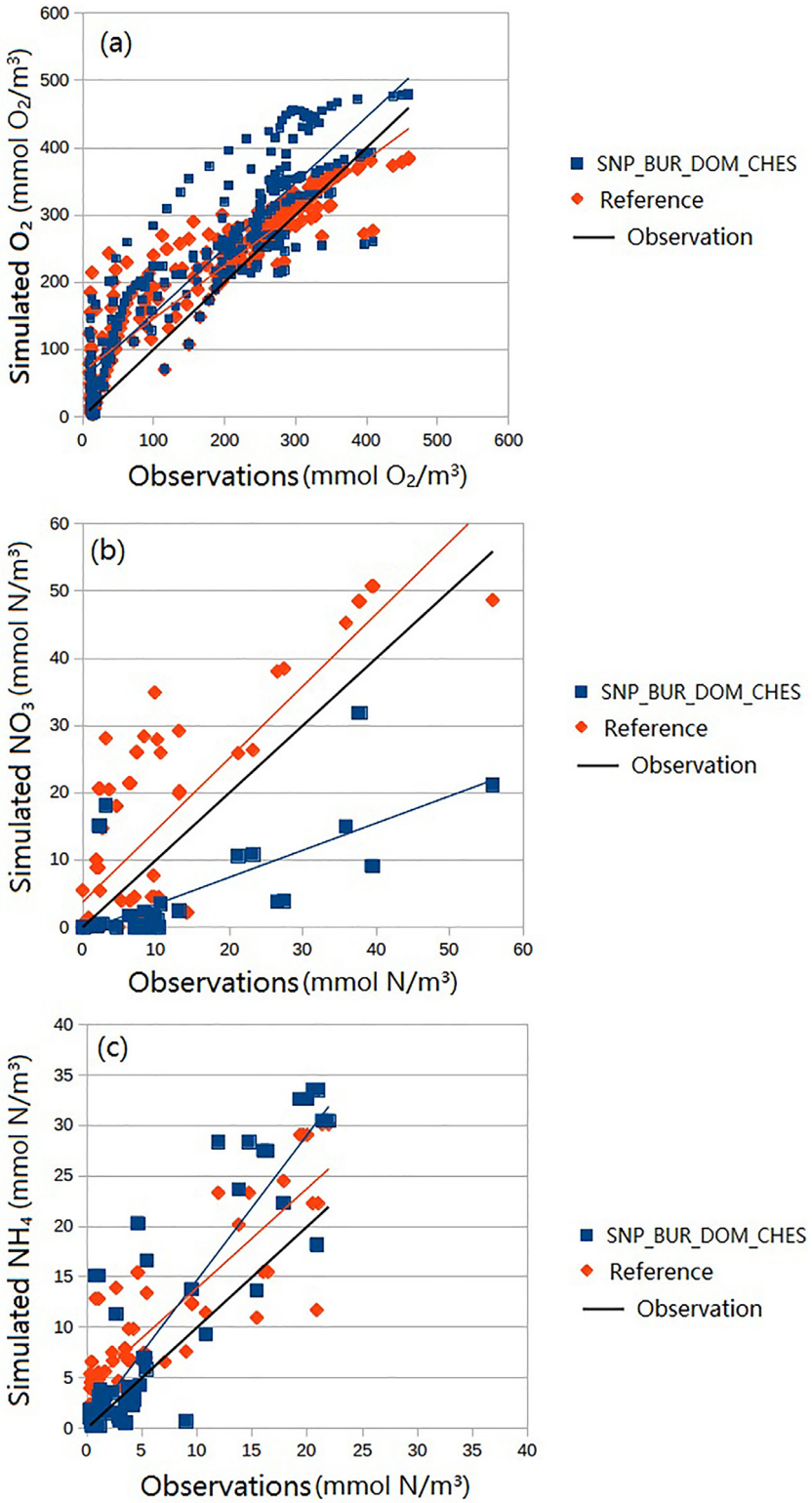


**Fig. 9.** Simulated versus observed oxygen (mmol $O_2/m^3$) (a) nitrate (mmol $N/m^3$) (b) and ammonium (mmol $N/m^3$) (c) at coincident times and locations from SNP_CHES_BUR_DON (blue) and new reference simulation which makes all three changes included in previous sensitivity runs (orange).

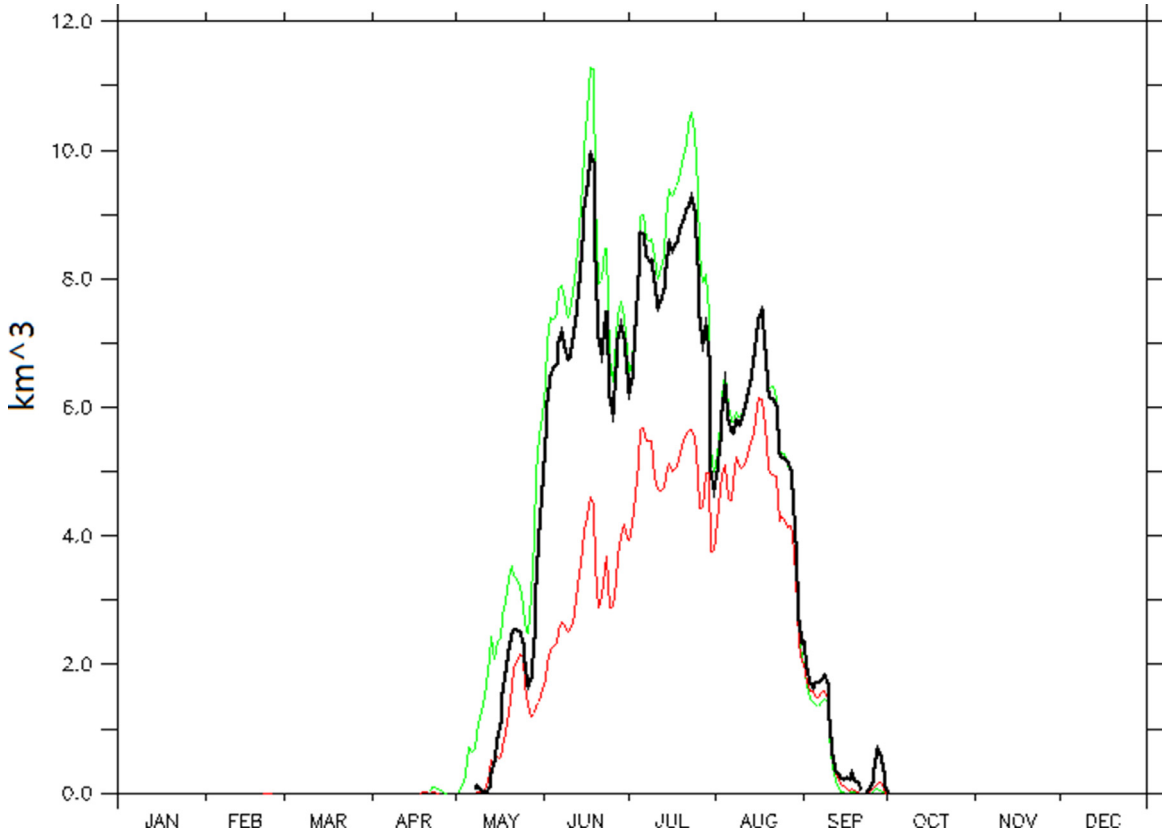


**Fig. 10.** Hypoxic volume simulated in N_BUR_DOM_CHES (VIMS hindcast, Black), SNP_BUR_DOM_CHES (red) and New reference (green).

## CRediT author statement

**Rui Jin:** Conceptualization, Methodology, Software, Investigation, Validity tests, Visualization, Data curation, Writing- Original draft preparation.**Marie-Aude Pradal**: Conceptualization, software, data curation, writing-original draft, writing-review and editing**. Kalev Hantsoo:** Software, writing-review and editing. **Anand Gnanadesikan:** Conceptualization, Methodology, Visualization, Writing-original draft preparation, writing-review and editing, supervision **Pierre St. Laurent:** Software, data curation, writing-review and editing. **Christian Bjerrum:** Software, writing-review and editing.

## Declaration of Competing Interest

The authors declare that they have no known competing financial interests or personal relationships that could have appeared to influence the work reported in this paper.

## Data availability

Data will be made available on request.

## Acknowledgments

This work was supported by
DOE Office of Science (SC0019344)
NOAA Climate Program Office (NA16OAR4310174)
The Johns Hopkins Institute for Data Intensive Engineering and Science (1201600132)
Danish National Research Foundation (DNRF 53)
Villum Foundation (grant 16518)

## References


[1] K. Arora-Williams, C. Holder, M. Secor, H. Ellis, M. Xia, A. Gnanadesikan, S.P. Preheim, Abundant and persistent sulfur-oxidizing microbial populations are responsive to hypoxia in the Chesapeake Bay, Environ. Microbiol. 24 (2022) 2315–2332, doi:10.1111/1462-2920.15976.

[2] M.Al Azhar, D.E. Canfield, K. Fennel, B. Thamdrup, C.J. Bjerrum, A model-based insight into the coupling of nitrogen and sulfur cycles in a coastal upwelling system, J. Geophys. Res. Biogeosci. 119 (2014) 264–285, doi:10.1002/2012JG002271.

[3] D.E. Canfield, F.J. Stewart, B. Thamdrup, L. De Brabandere, T. Dalsgaard, E.F. Delong, N.P. Revsbech, O. Ulloa, A Cryptic Sulfur Cycle in Oxygen-Minimum–Zone Waters off the Chilean Coast, Science (80-.). 330 (2010) 1375–1378, doi:10.1126/science.1196889.

[4] M. Cui, S. Adebayo, G. McPherson, K.H. Johannesson, Comparison of effects between kaolinite and hydrogen peroxide on tungsten and molybdenum speciation and implications for their geochemistry in aquatic environments, Chem. Geol. 582 (2021) 120418, doi:10.1016/j.chemgeo.2021.120418.

[5] F. Da, M.A.M. Friedrichs, P. St-Laurent, Impacts of Atmospheric Nitrogen Deposition and Coastal Nitrogen Fluxes on Oxygen Concentrations in Chesapeake Bay, J. Geophys. Res. Ocean. 123 (2018) 5004–5025, doi:10.1029/2018JC014009.

[6] Y. Feng, M.A.M. Friedrichs, J. Wilkin, H. Tian, Q. Yang, E.E. Hofmann, J.D. Wiggert, R.R. Hood, Chesapeake Bay nitrogen fluxes derived from a land-estuarine ocean biogeochemical modeling system: Model description, evaluation, and nitrogen budgets, J. Geophys. Res. Biogeosci. 120 (2015) 1666–1695, doi:10.1002/2015JG002931.

[7] K. Fennel, J. Wilkin, J. Levin, J. Moisan, J. O'Reilly, D. Haidvogel, Nitrogen cycling in the Middle Atlantic Bight: Results from a three-dimensional model and implications for the North Atlantic nitrogen budget, Glob. Biogeochem. Cycles 20 (2006) n/a-n/a, doi:10.1029/2005GB002456.

[8] K.G. Hantsoo, L.R. Kump, B.J. Haupt, T.J. Bralower, Tracking the Paleocene-Eocene Thermal Maximum in the North Atlantic: A Shelf-to-Basin Analysis With a Regional Ocean Model, Paleoceanogr. Paleoclimatol. 33 (2018) 1324–1338, doi:10.1029/2018PA003371.

[9] S.M. Henrichs, W.S. Reeburgh, Anaerobic mineralization of marine sediment organic matter: Rates and the role of anaerobic processes in the oceanic carbon economy, Geomicrobiol. J. 5 (1987) 191–237, doi:10.1080/01490458709385971.

[10] Jin, R., Pradal, M., Hantsoo, K., Gnanadesikan, A., St-laurent, P., 2023. Comparing two ocean biogeochemical models of Chesapeake Bay with and without the sulfur cycle instead highlights the importance of particle sinking, burial, organic matter, nitrification and light attenuation. Ocean Model. 182, 102175. https://doi.org/10.1016/j.ocemod.2023.102175.

[11] M.W. Lomas, P.M. Glibert, F.-K. Shiah, E.M. Smith, Microbial processes and temperature in Chesapeake Bay: current relationships and potential impacts of regional warming, Glob. Chang. Biol. 8 (2002) 51–70, doi:10.1046/j.1365-2486.2002.00454.x.

[12] R.A. Luettich, J.J. Westerink, N.W. Scheffner, ADCIRC: An Advanced Three-Dimensional Circulation Model for Shelves Coasts and Estuaries, Report 1: Theory and Methodology of ADCIRC-2DDI and ADCIRC-3DL, Dredging Research Program Technical Report DRP-92-6, Coast. Eng. Res. Cent. (U.S.), Eng. Res. Dev. Cent. (U.S.). (1992).

[13] G.W. Luther, T.M. Church, Seasonal cycling of sulfur and iron in porewaters of a Delaware salt marsh, Mar. Chem. 23 (1988) 295–309, doi:10.1016/0304-4203(88)90100-4.

[14] F. Mesinger, G. DiMego, E. Kalnay, K. Mitchell, P.C. Shafran, W. Ebisuzaki, D. Jović, J. Woollen, E. Rogers, E.H. Berbery, M.B. Ek, Y. Fan, R. Grumbine, W. Higgins, H. Li, Y. Lin, G. Manikin, D. Parrish, W. Shi, North American Regional Reanalysis, Bull. Am. Meteorol. Soc. 87 (2006) 343–360, doi:10.1175/BAMS-87-3-343.

[15] M.E. Scully, Mixing of dissolved oxygen in Chesapeake Bay driven by the interaction between wind-driven circulation and estuarine bathymetry, J. Geophys. Res. Ocean 121 (2016) 5639–5654, doi:10.1002/2016JC011924.

[16] A.F. Shchepetkin, J.C. McWilliams, Correction and commentary for "Ocean forecasting in terrain-following coordinates: Formulation and skill assessment of the regional ocean modeling system" by Haidvogel et al., J. Comp. Phys. 227, pp. 3595–3624, J. Comput. Phys. 228 (2009) 8985–9000, doi:10.1016/j.jcp.2009.09.002.

[17] A.F. Shchepetkin, J.C. McWilliams, The regional oceanic modeling system (ROMS): a split-explicit, free-surface, topography-following-coordinate oceanic model, Ocean Model. 9 (2005) 347–404, doi:10.1016/j.ocemod.2004.08.002.

[18] P.K. Smolarkiewicz, A Simple Positive Definite Advection Scheme with Small Implicit Diffusion, Mon. Weather Rev. 111 (1983) 479–486, doi:10.1175/1520-0493(1983)111<0479:ASPDAS>2.0.CO;2.

[19] P.K. Smolarkiewicz, L.G. Margolin, MPDATA: A Finite-Difference Solver for Geophysical Flows, J. Comput. Phys. 140 (1998) 459–480, doi:10.1006/jcph.1998.5901.